スケジュールが腫瘍により適切に設定可能であるが，精度がSRSより劣る可能性があり，さまざまな工夫が精度管理のためになされている．

定位放射線照射の治療成績は，局所制御において手術と同等と考えられている．有害反応はFlickingerら[5]の動静脈奇形に関する検討より，その発生頻度が照射部位によることが明らかとなり，照射部位や脳神経との位置関係により1回線量の低減が推奨されている．脳転移の治療は，全脳照射と手術に加え定位放射線照射の登場により，その選択の多様性と妥当性に関する検討がさまざまに行われている．

脳腫瘍の三次元放射線治療計画

小児の脳腫瘍ではAstrocytoma星細胞腫がもっとも多く，ついでMedulloblastoma髄芽腫，上衣腫やGerm Cell Tumorが続く．小児の脳腫瘍においては，手術や化学療法の併用による集学的治療の一環として放射線治療が応用されるが，遅発性放射線反応の軽減が重要な課題である．神経機能と神経内分泌機能の発達への影響を軽減するために，照射体積と照射線量の最適化をめざした試みがなされている．

Children's Oncology Group（COG）のLow-

表2　Intergroup Rhabdomyosarcoma Study Groupの臨床試験における横紋筋肉腫の放射線治療Guidelines

臨床試験	総　線　量	1回線量/ターゲット/タイミング	化学療法と結果
IRS Ⅰ (1972～78)	age＜3yrs＝40 Gy age＜6yrs and＜5 cm＝50 Gy age＞6 yrs or＞5 cm＝55 Gy age＞6 yrs and＞5 cm＝60 Gy	1.5～2.25 Gy/Fr/day whole muscle bundle or tumor＋margin no difference in local control Immediately:Groups Ⅰ and Ⅱ Week 6:Groups Ⅲ and Ⅳ	VAC, VA, VACA Overall 5-year survival 55%
IRS Ⅱ (1978～84)	Group Ⅰ＝no RT. Group Ⅱ＝40-45 Gy. Group Ⅲ：age＜6yrs and＜5 cm＝40-45 Gy age＞6 yrs or＞5 cm＝45-50 Gy age＞6 yrs and＞5 cm＝50-55 Gy	1.5～2.25 Gy/Fr/day GTV＋2 cm Week 0:Group Ⅱ Week 6:Groups Ⅲ and Ⅳ	VAC, VA, VadrC-VAC Overall 5-year survival 63% Botryoid89%, Embryonal 68%, Alveolar 52%, Other 55%
IRS Ⅲ (1984～88)	Grp Ⅰ FH-no RT. Grp Ⅰ UH/Ⅱ-41.4 Gy. Group Ⅲ varied by age, size but all＜50.4 Gy.	GTV＋2 cm Day 0:PM with CN palsy, BOS erosion, intracranial extension. Week 2:Group Ⅱ FH/Group Ⅲ orbit and H/N. Week 6:all others	VAC, VA, VadrC-VAC, VAadr CDDP/VP16 VadrC-VAC＋CDDP Overall 5-year survival 71%
IRS Ⅳ (1991～97)	Group Ⅰ, Stage 1/2-no RT. Group Ⅰ, Stage3/Ⅱ-41.4 Gy CRT. Group Ⅲ randomized to 50.4 Gy CRT vs 59.4 Gy HRT（1.1 Gy BID）	GTV＋2 cm Day 0:PM with CN palsy, BOS erosion, intracranial extension. Week 12:all others	VA, VAC, VAI, VIE Overall 3-yr FFS 77% No difference in local control with CRT vs HRT.
IRS Ⅴ (1999～04)	Experimental dose reductions for selected patients: Group Ⅰ alveolar/undifferentiated 36 Gy Group Ⅱ N0:36 Gy Group Ⅲ orbit/eyelid:45 Gy Group Ⅲ second look surgery negative margins:36 Gy microscopically＋margins:41.4 Gy Group Ⅲ requiring 50.4Gy: volume reduction to initial GTV＋5 mm at 36 Gy if N0, and at 41.4 Gy if N＋	GTV＋2 cm Day 0:PM with intracranial extension only Week 3:low risk, week 12:intermediate, week 15:high risk	Low risk:VA, VAC Intermediate Risk: VAC vs VAC/VTC

Grade Glioma に対する臨床試験においては[6)~7)]，3D-CRT が応用され線量分布の改善による遅発性放射線反応の軽減が図られている．小児の Glioma の治療においては，発達への影響を考慮して放射線治療の適応を躊躇する傾向にあったが，3D-CRT による正常組織への影響の軽減によって，放射線治療のより積極的な応用が検討されており，今後の臨床試験結果が注目される．

Medulloblastoma の集学的治療においては，Craniospinal Irradiation（CSI）が標準治療であり，high risk 群で 36 ～ 40 Gy，average risk 群で 18 ～ 24 Gy 程度の CSI と，54 Gy 前後の後頭蓋窩への照射が組み合せて施行されている．Children's Cancer Group（CCG）で施行された CCG9892 では，化学療法の併用により CSI の線量を低減する臨床試験が施行され，その効果が確認された[8)]．その後の CCG9961 では average risk 群では，化学療法併用で 23.4Gy の CSI と 54 ～ 55.8 Gy の後頭蓋窩への照射が施行された．さらに COG では，average risk 群で CSI の線量の低減とともに，3D-CRT を応用して原発巣への追加照射の照射野を，後頭蓋窩より腫瘍床＋margin へ限局する臨床試験が提案されている．総線量や照射野以外に考慮されるべき放射線治療因子として，治療期間の延長が治療効果に与える影響が delCharco らにより報告されている[9)]．5 年後頭蓋窩制御率が照射期間 45 日以内で 89％であったのに対し，45 日を超えると 68％と低下し（p ＝ 0.01），5 年無再発生存率が照射期間 45 日以内で 76％であったのに対し，45 日を超えると 43％と低下していた（p ＝ 0.004）．放射線治療の中断の治療効果への影響は，International Society of Paediatric Oncology（SIOP）と United Kingdom Children's Cancer Study Group（UKCCSG）の臨床試験でも指摘されており[10)]，今後臨床試験を検討する際に十分認識すべきと考える．

軟部組織腫瘍の三次元放射線治療計画

横紋筋肉腫の治療は，1970 年代より集学的治療が積極的に進められており，臨床試験の結果により治療成績の改善が進められてきた分野の一つである．表 2 に，Intergroup Rhabdomyosarcoma Study Group により計画されてきた集学的治療の経過を示す[11)~15)]．放射線治療は，化学療法の併用薬剤の変化とともに総線量の軽減が図られた．一方で，IRS-Ⅳでは Group Ⅲにおいて，50.4 Gy の通常分割照射と 59.4 Gy の多分割照射（1.1 Gy を 1 日 2 回照射）が比較検討された．Donaldson らの報告では[16)]，failure-free survival（FFS）および overall survival（OS）と

表 3　IRS-V 放射線治療 Guidelines による正常組織の耐容線量と DVH による評価

正常組織		通常照射による上限	DVH
頭部	脳	全脳 3 歳未満 23.4Gy	不要
		全脳 3 歳以上 30.6Gy	不要
	左右網膜		必要
	左右視神経	46.8Gy	必要
	視神経交叉	46.8Gy	必要
	下垂体		必要
	角膜	41.4Gy	不要
	水晶体	14.4Gy	不要
	涙腺	41.4Gy	不要
	蝸牛		必要
頸部	甲状腺		必要
胸部	肺	両肺 14.4Gy	必要
	心臓	全心臓 30.6Gy	必要
腹部	肝臓	全肝 23.4Gy	必要
	腎臓	両側で 14.4Gy	必要
	消化管	一部 45Gy	不要
	全腹―骨盤	30Gy（1.5Gy/回）	不要
骨盤	膀胱		必要
	直腸		必要
脊髄	脊髄	45Gy	必要

この耐容線量は化学療法と併用した場合の有害事象の増強することが考慮されていない．大量化学療法併用時の耐容線量はさらに低いことが予想され，両側腎，肝臓全体，両側肺，全脳，脊髄，心臓全体への照射の場合はさらに 5 Gy 程度低い線量を上限とすることが望ましいと考えられる

もに通常分割照射と多分割照射で有意差を認めなかった．現在進行中のIRS-Vでは，1日1回1.8 Gy/回の通常分割照射が採用され，新たにIMRTを含む3D-CRTが推奨されており，小線源治療や陽子線治療を含む正常組織の線量を軽減した放射線治療が，放射線治療ガイドラインに取り入れられている．**表3**にIRS-Vの放射線治療Guidelinesにおいて示されている正常組織の耐容線量とDVHによる評価が必要な正常組織を示す．今後，臨床試験の結果によるevidenceの蓄積により，さらに適切な照射線量の設定が可能となることが期待されている．

おわりに

小児の悪性腫瘍において，放射線治療の技術的進歩により応用範囲が拡大してきている．小児に対する放射線治療は，リスク臓器の線量に細心の注意をはらった治療が実施されるべきであり，さらに有害事象の経過観察が長期に必要である．

今後，線量分布の最適化による治療成績の向上と有害事象の軽減や，分割照射方法や化学療法や手術との併用の工夫に関するevidenceの蓄積が求められている．

●文　献

1) 永田　靖，平岡真寛：三次元放射線治療計画（IMRTを含む）．平岡真寛，笹井啓資，井上俊彦・編，放射線治療マニュアル，中外医学社，東京，45-60, 2001
2) International Commission on Radiation Units and Measurements Report 62, Prescribing, Recording and Reporting Photon Beam Therapy（Supplement to ICRU Report 50）. ICRU Publications, 1999
3) Morita K: Conformal RT and conformation RT. Int J Radiation Oncology Biol Phys 48: 431-434, 2000
4) Leksell L: Stereotactic radiosurgery. J Neurol Neurosurg Psychiatry 46（9）: 797-803, 1983
5) Flickinger JC, Kondziolka D, Maitz AH et al.: Analysis of neurological sequelae from radiosurgery of arteriovenous malformations: how location affects outcome. Int J Radiat Oncol Biol Phys 40（2）: 273-278, 1998
6) Wisoff JH, Sanford A, Sposto R et al.: Low grade gliomas of childhood: Impact of surgical resection-A report from the Children's Oncology Group protocol CCG-9891/POG-9130. J Neurosurg 96: 427-428, 2002
7) Shaw EG, Wisoff JH: Prospective clinical trials of intracranial low-grade glioma in adults and children. Neuro-Oncology,（in Press）
8) Packer RJ, Goldwein J, Nicholson HS et al.: Treatment of children with medulloblastomas With Reduced-Dose craniospinal radiation therapy and adjuvant chemotherapy: A Children's Cancer Group Study J Clin Oncol 17: 2127-2136, 1999
9) DelCharco JO, Bolek TW, McCollough WM et al.: Medulloblastoma: Time-dose relationship based on a 30-year review. Int J Radiation Oncology Biol Phys 42: 147-154, 1998
10) Taylor RE, Bailey CC, Robinson K et al.: Results of a randomized study of preradiation chemotherapy versus radiotherapy alone for nonmetastatic medulloblastoma: The International Society of Paediatric Oncology/United Kingdom Children's Cancer Study Group PNET-3 Study J Clin Oncol 21: 1581-1591, 2003
11) Wolden SL, Anderson JR, Crist WM et al.: Indications for radiotherapy and chemotherapy after complete resection in Rhabdomyosarcoma: A Report From the Intergroup Rhabdomyosarcoma Studies Ⅰ to Ⅲ. J Clin Oncol 17: 3468-3475, 1999
12) Maurer H, Beltangady M, Gehan E et al.: The Intergroup Rhabdomyosarcoma Study-Ⅰ: A final report. Cancer 61: 209-220, 1988
13) Maurer H, Gehan E, Beltangady M et al.: The Intergroup Rhabdomyosarcoma Study-Ⅱ. Cancer 71: 1904-1922, 1993
14) Crist W, Gehan EA, Ragab AH et al.: The third Intergroup Rhabdomyosarcoma Study. J Clin Oncol 13: 610-630, 1995
15) Crist WM, Anderson JR, Meza JL et al.: Intergroup

rhabdomyosarcoma study-Ⅳ: Results for patients with nonmetastatic disease. J Clin Oncol 19: 3091-3102, 2001
16) Donaldson SS, Meza J, Breneman JC et al.: Results from the IRS-IV randomized trial of hyperfractionated radiotherapy in children with rhabdomyosarcoma-A report from the IRSG. Int J Radiation Oncology Biol Phys 51: 718-728, 2001

著者連絡先
〒104-0045 東京都中央区築地5-1-1
国立がんセンター中央病院放射線治療部
角美奈子

Neuro-Oncology

Mechanisms of action of rapamycin in gliomas[1]

Amy B. Heimberger,[2] Enze Wang, Eric C. McGary, Kenneth R. Hess, Verlene K. Henry, Tadahisa Shono, Zvi Cohen, Joy Gumin, Raymond Sawaya, Charles A. Conrad, and Frederick F. Lang

Brain Tumor Center and Departments of Neurosurgery (A.B.H., E.W., V.K.H., T.S., Z.C., J.G., R.S., F.F.L.), Biostatistics (K.R.H.), and Neuro-Oncology (C.A.C.), The University of Texas M.D. Anderson Cancer Center, Houston, TX 77030; Hilton Head Regional Medical Center, Hilton Head, SC 29926 (E.C.M.); USA

Rapamycin has previously been shown to be efficacious against intracerebral glioma xenografts and to act in a cytostatic manner against gliomas. However, very little is known about the mechanism of action of rapamycin. The purpose of our study was to further investigate the in vitro and in vivo mechanisms of action of rapamycin, to elucidate molecular end points that may be applicable for investigation in a clinical trial, and to examine potential mechanisms of treatment failure. In the phosphatase and tensin homolog deleted from chromosome 10 (PTEN)-null glioma cell lines U-87 and D-54, but not the oligodendroglioma cell line HOG (PTEN null), doses of rapamycin at the IC_{50} resulted in accumulation of cells in G_1, with a corresponding decrease in the fraction of cells traversing the S phase as early as 24 h after dosing. All glioma cell lines tested had markedly diminished production of vascular endothelial growth factor (VEGF) when cultured with rapamycin, even at doses below the IC_{50}. After 48 h of exposure to rapamycin, the glioma cell lines (but not HOG cells) showed downregulation of the membrane type–1 matrix metalloproteinase (MMP) invasion molecule. In U-87 cells, MMP-2 was downregulated, and in D-54 cells, both MMP-2 and MMP-9 were downregulated after treatment with rapamycin. Treatment of established subcutaneous U-87 xenografts in vivo resulted in marked tumor regression ($P < 0.05$). Immunohistochemical studies of subcutaneous U-87 tumors demonstrated diminished production of VEGF in mice treated with rapamycin. Gelatin zymography showed marked reduction of MMP-2 in the mice with subcutaneous U-87 xenografts that were treated with rapamycin as compared with controls treated with phosphate-buffered saline. In contrast, treatment of established intracerebral U-87 xenografts did not result in increased median survival despite inhibition of the Akt pathway within the tumors. Also, in contrast with our findings for subcutaneous tumors, immunohistochemistry and quantitative Western blot analysis results for intracerebral U-87 xenografts indicated that there is not significant VEGF production, which suggests possible deferential regulation of the hypoxia-inducible factor 1α in the intracerebral compartment. These findings demonstrate

Received April 29, 2004; accepted June 29, 2004.

[1] Supported by The University of Texas M.D. Anderson Cancer Center National Institutes of Health Core Grant P30 CA16672, the Bullock Research Foundation, and the Elias Family Fund for Brain Tumor Research.

[2] Address correspondence to Amy B. Heimberger, Department of Neurosurgery, The University of Texas M.D. Anderson Cancer Center, Unit 442, 1515 Holcombe Boulevard, Houston, TX 77030-4009, USA (aheimber@mdanderson.org).

[3] Abbreviations used are as follows: BSA, bovine serum albumin; CD3, T cell type I transmembrane protein; EDTA, ethylenediamine tetraacetic acid; ELISA, enzyme-linked immunosorbent assay; FCS, fetal calf serum; FRAP, FKBP-rapamycin-associated protein; HIF, hypoxia-inducible factor; IC_{50}, inhibitory concentration 50; IL-2, interleukin 2; MMP, matrix metalloproteinase; MT1, membrane type–1; mTOR, mammalian target of rapamycin; PAGE, polyacrylamide gel electrophoresis; PI3K, PI3 kinase; PBS, phosphate-buffered saline; PTEN, phosphatase and tensin homolog deleted from chromosome 10; SDS, sodium dodecyl sulfate; SPF, sterile, pathogen free; VEGF, vascular endothelial growth factor.

[4] Personal communication, Candelaria Gomez-Manzano, M.D. Anderson Cancer Center, September 15, 2004.

that the complex operational mechanisms of rapamycin against gliomas include cytostasis, anti-VEGF, and anti-invasion activity, but these are dependent on the in vivo location of the tumor and have implications for the design of a clinical trial. *Neuro-Oncology 7, 1–11, 2005 (Posted to Neuro-Oncology [serial online], Doc. 04-042, November 17, 2004. URL http://neuro-oncology.mc.duke.edu; DOI: 10.1215/S1152851704000420)*

Classic phase 1 and 2 clinical trials determine the safety and efficacy of agents by evaluating indirect end points based on clinical assessments of toxicity and response, respectively. Reliance on these indirect end points leaves unanswered important questions such as whether the drug actually reaches the tumor and whether it alters the biology of the tumor. Consequently, investigators have proposed revising the standard clinical design of brain tumor trials to also include assessments of molecular targets to optimize dose and to determine efficacy (Lang et al., 2002). For these trials to be successful, however, preclinical studies must be aimed at defining the appropriate molecular end points and developing clinically applicable assays to assess these end points (Lang et al., 2002). A molecular approach makes more efficient use of animal studies given the frequent observation that efficacy in animals only rarely correlates with efficacy in humans. Because several groups have proposed evaluating rapamycin, or one of its derivatives, as a potential treatment for patients with malignant gliomas, we explored the molecular targets of rapamycin in order to determine which ones could be used as end point(s) in molecular target–based, early-phase clinical trials.

Rapamycin has been recognized as an antineoplastic agent and is a potent inhibitor of tumor cell growth (Sehgal et al., 1975; Supko and Malspeis, 1994), specifically inhibiting the Ser-Thr kinase activity of mammalian target of rapamycin (mTOR)[3] FKBP-rapamycin-associated protein (FRAP) (Neshat et al., 2001; Price et al., 1992), a signaling molecule that links extracellular signaling to protein translation (Dilling et al., 1994). Activation of growth factor or cytokine receptors results in the sequential activation of PI3 kinase (PI3K), PDK1, Akt/PKB, and mTOR-FRAP. Treatment of cells with rapamycin leads to the dephosphorylation and inactivation of p70S6 kinase and 4EBP1. Dephosphorylation of 4EBP1 results in the binding to e1F4E, which inhibits translation. The tumor suppressor phosphatase and tensin homolog deleted from chromosome 10 (PTEN) downregulates Akt activity, and PTEN-null cell lines expressing high levels of Akt, such as U-87, U-251, SF-539, and SF-295, are sensitive to rapamycin inhibition of mTOR-FRAP at an IC_{50} of less than 0.01 μM in vitro (Neshat et al., 2001). Although in established subcutaneous U-87 glioma tumors, doses of rapamycin that inhibit mTOR (1 mg/kg administered i.p. once every 3 days) are insufficient for suppression of growth (Eshleman et al., 2002), higher doses of rapamycin (1.5 mg/kg administered i.p. once daily) inhibit tumor growth and angiogenesis (Guba et al., 2002). Furthermore, rapamycin has been shown to be efficacious against established intracerebral U-251 gliomas in a murine model. Specifically, mice treated with rapamycin intraperitoneally at 200, 400, and 800 mg/kg/injection had increased life spans of 67%, 47%, and 78%, respectively, compared to survival of untreated controls (Houchens et al., 1983), suggesting that rapamycin may be a promising agent against gliomas.

The purpose of our study was to further investigate the in vitro and in vivo mechanisms of action of rapamycin in order to elucidate molecular end points that may be applicable in early phase clinical trials and to examine potential mechanisms of treatment failure. This study demonstrates that rapamycin affects cytostasis, cell signaling, angiogenesis, and invasion in vitro. Although rapamycin in our model system demonstrated in vivo efficacy in the subcutaneous compartment, an increase in median survival was not seen in the intracerebral compartment, which indicates that the anatomical microenvironment influences the tumor response to rapamycin.

Materials and Methods

Tumor Cell Lines

The cell lines U-87, D-54, and HOG (provided for our study as a gift) are PTEN null and were maintained in Dulbecco's Modified Eagle Medium/F12 medium (Mediatech, Inc., Herndon, Va.) supplemented with 10% fetal bovine serum (GIBCO-BRL, Rockville, Md.). All cell lines tested negative for *Mycoplasma* contamination. Both U-87 and D-54 express high constitutive levels of hypoxia-inducible factor (HIF)-1α,[4] resulting in enhanced expression of vascular endothelial growth factor (VEGF).

Drugs

Rapamycin (sirolimus; Sigma Chemical Co., St. Louis, Mo.) and its derivative RAD001 [everolimus; 40-O-(2-hydroxyethyl)-rapamycin; Novartis Institutes of Biomedical Research, Novartis Pharma AG, Basel, Switzerland] were stored at a concentration of 5 mg/ml and 10^{-2} M, respectively, in 100% ethanol at –20°C and were diluted in serum-free medium immediately prior to use. The oral formulation of RAD001 is provided as a microemulsion preconcentrate that has efficacy after oral dosing equivalent to that of rapamycin and has the same mode of action at the cellular and molecular level as rapamycin (Schuler et al., 1997). When compared to rapamycin, the in vitro activity of RAD001 is generally about two to three times lower (Schuler et al., 1997).

Murine Models and Tumor Formation

All animal studies were conducted with a protocol approved by the Institutional Animal Care and Use Committees. Male 6- to 8-week-old nude mice (The Jackson Laboratory, Bar Harbor, Maine) were housed within an approved specific pathogen–free barrier facility maintained at the M.D. Anderson Isolation Facility in accordance with Laboratory Animal Resources Com-

mission standards. Appropriate measures were taken to minimize animal discomfort, and appropriate sterile surgical techniques were utilized in tumor implantation and drug administration. Animals that became moribund or had necrotic tumors were compassionately euthanized.

To induce the subcutaneous tumors, logarithmically growing U-87 cells were injected into the right hind flank of nude mice at a dose of 1×10^6 cells per 200 μl. Treatment with rapamycin intraperitoneally at a dose of 1.5 mg/kg/day was begun when the majority of animals had palpable tumors (at day 5). Tumors were measured every other day, and tumor volumes (length × width^2/2) were calculated on the basis of the tumors that grew in surviving mice.

To induce intracerebral tumor, U-87 cells (5×10^5) were engrafted into the caudate nucleus of athymic mice as previously described (Lal et al., 2000). We performed three independent experiments using 6 to 10 animals per group in each experiment. For the survival studies, treatment was started on day 3 after implantation of the U-87 cells, and mice were treated via oral gavage with RAD001, the derivative of rapamycin. To obtain tumors of sufficient size to perform the biological assays, treatment was started on day 7 after implantation of U-87 cells.

In Vitro Cytotoxicity

Cells in logarithmic growth at 80% confluency were harvested with trypsin-EDTA (0.5–0.2 g/liter) solution (GIBCO-BRL), washed with phosphate-buffered saline (PBS), and plated in triplicate in 96-well U-bottom plates at a concentration of 2×10^4 cells/ml. Rapamycin was added at concentrations of 0, 0.001, 0.01, 0.1, 1.0, 10, 100, and 1000 ng/ml, and the plates were incubated at 38°C for 24 h. Counts of viable cells were determined by the trypan blue dye exclusion method.

Cell Cycle Analysis

Cells in logarithmic growth at a concentration of 1.5×10^6 cells/ml were treated with rapamycin at doses of 0, 0.1, 1.0, and 10 ng/ml for U-87 cells; 0, 1.0, 10, and 100 ng/ml for D-54 cells; and 0, 100, and 1000 ng/ml for HOG cells. Cells were fixed with 70% ethanol, stained with 20 μg/ml of propidium iodide and 100 μg/ml of RNase A, and incubated at 37°C for 30 min. Flow cytometric analysis was performed with appropriate gating on a FACScan (Becton Dickinson Immunocytometry Systems, San Jose, Calif.).

Western Blot Analysis

Cell lines or minced tumor tissue underwent protein extraction in 20 mM Tris-HCl, pH 8.0, 137 mM NaCl, 10% glycerol, 0.1% sodium dodecyl sulfate (SDS), leupeptin 0.2 μg/ml, aprotinin 5 μg/ml, phenylmethyl sulfonyl fluoride 1 mM (Sigma), and 1% NP-40 (Amersham, Piscataway, N.J.) for 15 min at 4°C. The supernatant was stored at −70°C after centrifugation. Protein concentration was determined by standard Bio-Rad protein assay (Bio-Rad, Hercules, Calif.). Equivalent amounts of protein extracts (20 μg/well) were subjected to 12.5% SDS–polyacrilamide gel electrophoresis (PAGE) gel denaturing conditions and were immunoblotted with anti-VEGF (Sigma), anti–matrix metalloproteinase 2 (MMP-2) (Sigma), anti-4EBP1 (Cell Signaling Technology, San Jose, Calif.), anti-α-tubulin (Sigma), or anti-β-actin (Sigma). Fold increases in intensity of each band were scanned with a densitometer (Molecular Dynamics, Piscataway, N.J.), normalized to control β-actin or α-tubulin, and analyzed by using ImageQuant (Molecular Dynamics).

Vascular Endothelial Growth Factor Enzyme-Linked Immunosorbent Assay

The glioma cells were treated with rapamycin in serum-free medium as previously described. Cell viability at the completion of the experiment was determined by trypan blue exclusion. The medium was collected and stored at −80°C and was not subjected to more than one freeze-thaw cycle prior to use. VEGF secretion was measured in duplicate samples by enzyme-linked immunosorbent assay (ELISA) according to the manufacturer's instructions (R & D Systems, Minneapolis, Minn.).

Immunohistochemistry

Tumors removed from nude mice were fixed in 10% formalin solution for approximately 6 h at room temperature and then embedded in paraffin. Sections of paraffin-embedded tumors were deparaffinized in xylene, rehydrated, and then stained after endogenous peroxidase was inactivated by treating them with 3% H_2O_2 for 5 min at room temperature. Tissue staining was performed with the HRB-DAB system (R & D Systems) according to the manufacturer's instructions. The primary antibodies utilized were mouse anti-human VEGF (R & D Systems) at a 1:50 dilution or mouse anti-human membrane type–1 (MT1)-MMP (R & D Systems) at a 1:22 dilution. The slides were counterstained with hematoxylin, and the tumor sections were examined with a Nikon microscope.

Gelatin Zymography

The supernatant from glioma cell lines treated with medium containing rapamycin or medium alone was harvested and stored at −80°C prior to use. The samples (each containing 15 μg of supernatant protein) were fractionated by electrophoresis on a polyacrylamide gel containing 10% SDS and gelatin (Bio-Rad). To determine in vivo MMP activity, tumor fragments (10 mm^3 each) were cut from the tumor, weighed, and extracted with 2 × SDS sample buffer (1:2 w/v). After extraction for 2 h at room temperature, samples were diluted 2-fold with 1 × SDS sample buffer and homogenized by repeated pipetting. The solubilized material was separated from the pellet by centrifugation at 14,000 × *g* for 30 min, and aliquots of these supernatants were analyzed by gelatin zymography (20 μl/sample lane). Coo-

massie blue staining confirmed equivalent protein loading of samples on gels.

SDS was subsequently removed from the gels with 2.5% Triton X-100, and they were incubated overnight at 37°C in a solution containing 50 mM Tris base, 200 mM NaCl, 5 mM $CaCl_2$, and 0.02% Brij-35 (30%). The gels were then stained with 0.5% Coomassie blue in 40% methanol and 10% acetic acid for 2 h at room temperature with agitation and then destained with 40% methanol and 10% acetic acid to reveal clear bands of proteolytic activity.

MT1-MMP Analysis

Cell lines treated as previously described with rapamycin or media alone were washed with PBS containing 1% bovine serum albumen (BSA) and stained for 40 min with 10 μg/ml of rabbit control IgG or an antibody against the hinge domain of MT1-MMPs (Sigma). After washing, the cells were stained with the secondary fluorescein isothiocyanate–conjugated $F(ab')_2$ fragment of goat anti-rabbit IgG (Sigma) for 30 min. Cells were analyzed on a Becton Dickinson FACScan with cell population gates for negative control set by using cells stained with rabbit IgG.

Cell Invasion Assay

Tumor cell invasion was measured with Matrigel Invasion Chambers (BD Biosciences, San Jose, Calif.). The glioma cell lines in 5% fetal calf serum (FCS) were added at a concentration of 5×10^4 to the upper chamber, and 10% FCS was used in the lower chamber to induce cell migration. Rapamycin was added to the upper chamber at concentrations spanning the IC_{50}. Duplicate filters were used for each treatment, and all the cells on each filter were counted by using an inverted microscope.

Statistical Analysis

Spearman rank correlation coefficient analysis was used to analyze the VEGF ELISA data. A linear model relating the VEGF values to log dose, time, and cell line was used to include a three-way interaction as well as all nested two-way interactions. Residual analyses demonstrated that the model fit the data. A two-sample *t* test assuming equal variances between groups was used to determine the statistical significance on quantitative Western blot densitometry. The nonparametric Wilcoxon rank sum test was used to compare the volumes of subcutaneous tumors between rapamycin-treated and untreated groups. Statistical significance was determined as $P < 0.05$.

Results

In Vitro Studies

Determination of IC_{50} of rapamycin for glioma cell lines. To determine whether there was a direct cytostatic effect of rapamycin on the growth of U-87, D-54, and HOG cells, these lines in logarithmic growth were exposed to 0 to 1000 ng/ml of rapamycin. After 24 h, the cells were harvested and counted; the IC_{50} for U-87, D-54, and HOG was 0.65, 75, and >1000 ng/ml of rapamycin, respectively.

Table 1. Flow cytometric analysis results showing rapamycin-induced G_1 arrest in D-54 and U-87 glioma cells but not in HOG oligodendroglioma cells*

Cell Line	Time	Rapamycin Dose (ng/ml)	% Sub-G_0/G_1	% G_1	% G_2	% S
D-54	24	0	<1	52.4	10.7	36.9
D-54	24	100	<1	64.3	9.4	26.2
D-54	48	0	<1	40.3	16.1	43.6
D-54	48	10	<1	68.1	5.6	26.4
U-87	24	0	<1	47.0	8.2	44.7
U-87	24	1	<1	59.2	32.3	8.5
U-87	48	0	<1	57.7	25.1	17.2
U-87	48	100	<1	67.8	24.4	7.8
HOG	24	0	<1	38.3	31.1	30.6
HOG	24	1000	<1	35.2	27.2	37.6
HOG	48	0	<1	55.1	28.7	16.2
HOG	48	1000	<1	52.6	26.8	20.6

* Cell lines were treated with rapamycin at the IC_{50} for 24 h, the DNA content was measured by flow cytometry after cells were stained with propidium iodide, and the proportions of cells in G_1, G_2, and S phases of the cell cycle were computed. The experiment was replicated twice at two different time points with similar results.

Rapamycin induces G_1 arrest in glioma cell lines. To determine if rapamycin induced cell cycle arrest, D-54, U-87, and HOG cell lines were treated for 24 and 48 h with medium alone or with medium containing rapamycin at the respective IC_{50} dose determined for each line. Flow analysis cytometry was performed to determine the fraction of cells in subG_0/G_1 (apoptosis), G_1, G_2, and S phases (Table 1). Treatment of the D-54 and U-87 cell lines with rapamycin resulted in the accumulation of cells in the G_1 compartment, indicating that rapamycin acts in a cytostatic manner. Treatment of the HOG cell line, even with maximum doses of rapamycin, failed to induce cytostasis.

RAD001 (everolimus) suppresses the phosphorylation of p-4EBP1, a downstream signal molecule of the Akt pathway. To determine whether the rapamycin derivative RAD001 could decrease the phosphorylation of the downstream signaling molecule p-4EBP1 of the Akt pathway, U-87 cells were cultured for 24 h with doses of RAD001 spanning the IC_{50}, and the amount of p-4EBP1 was quantitated on Western blot. With volumetric band density normalized to a maintenance protein (α-tubulin), RAD001 significantly diminished production of p-4EBP1 (Fig. 1A). This data is consistent with previously published reports that the Akt pathway is inhibited by rapamycin.

Rapamycin suppresses the secretion of VEGF in glioma cell lines. To determine whether rapamycin could

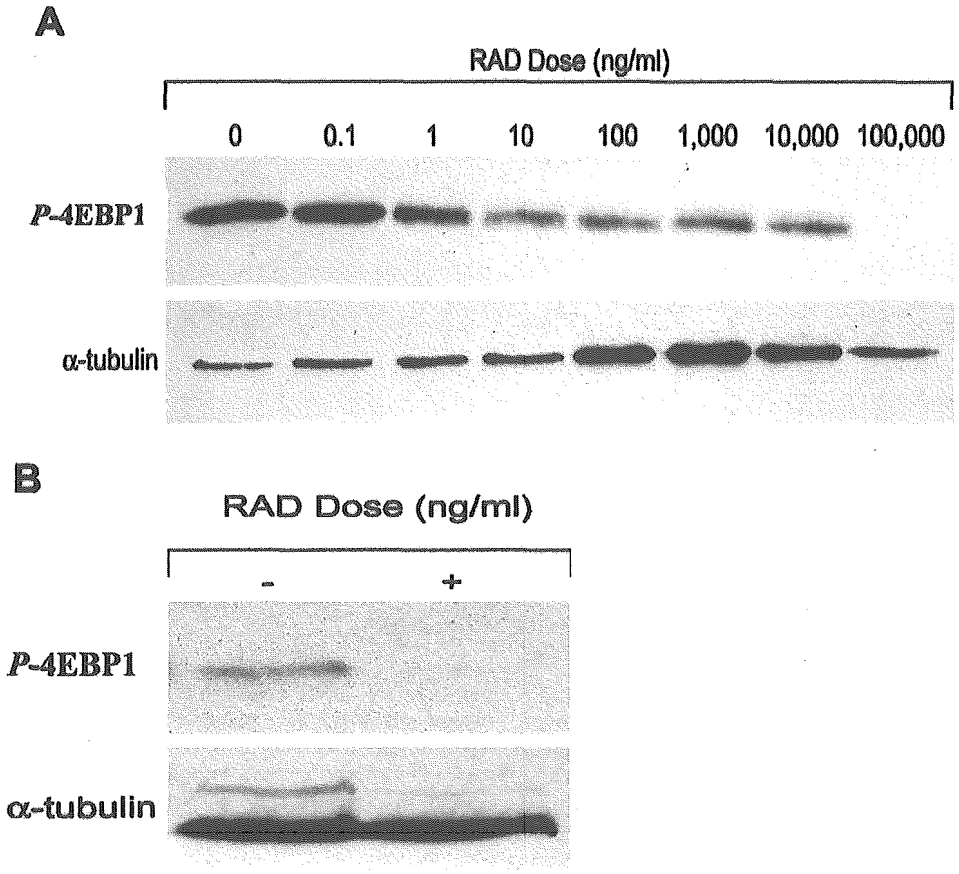

Fig. 1. Quantitative Western blot analysis demonstrating inhibition of p-4EBP1 by RAD001. U-87 (A) or U-87 intracerebral tumors (B) were treated with the derivative of rapamycin, RAD001, as described in the Materials and Methods section. Equivalent amounts of protein extracts (20 μg/well) were subjected to 12.5% SDS-PAGE gel denaturing conditions and were immunoblotted with anti-4EBP1 and anti-α-tubulin. Fold increases in intensity of each band were scanned with a densitometer and normalized to control α-tubulin. RAD001 inhibited the phosphorylated form of 4EBP1, the downstream signaling molecule of Akt, both in vitro and in vivo.

decrease the production of VEGF in vitro, we cultured glioma cells for 24 and 48 h with doses of rapamycin spanning the IC_{50}, and we determined the VEGF concentration by ELISA. To control for the effect of diminished cell number as the basis for diminished VEGF production, cell counts at each time point were determined, and VEGF secretion per cell was calculated. At 24 and 48 h there was a markedly diminished production of VEGF by all glioma cell lines at rapamycin doses significantly below the IC_{50}. Even though an IC_{50} could not be determined for the HOG cell line, dramatic inhibition of VEGF production was seen after 48 h of exposure to rapamycin at 10 ng/ml (Fig. 2).

Rapamycin inhibits invasion and downregulates MMPs. The enzymatic activities of MT1-MMP and MMP-2 contribute to the integrity of the extracellular matrix in the brain, and hydrolysis of the brain's extracellular matrix allows glioma cells to invade normal brain tissue. To determine whether rapamycin downregulates MMPs, we treated the cell lines U-87, D-54, and HOG in vitro with rapamycin for 48 h, and we used flow cytometry to quantify the amount of the membrane-bound MMP, MT1-MMP, after the cell line had been exposed to a monoclonal antibody to MT1-MMP (see Materials and Methods). After 48 h of treatment with 10 ng/ml and 100 ng/ml of rapamycin, respectively, the glioma cell lines U-87 and D-54 showed downregulation of MT1-MMP (Table 2). In contrast, there were minimal levels of MT1-MMP expressed in the HOG cell lines, which did not appear to be affected by treatment with 1000 ng/ml of rapamycin (data not shown).

Because MT1-MMP-expressing glioma cells can activate proMMP-2, with the resulting enzymatic activity of MMP-2 facilitating tumor invasion of normal brain, we determined if rapamycin downregulated the secretory invasion molecules MMP-2 and MMP-9. The glioma cell lines were treated with rapamycin for 48 h, and for each cell line, the supernatant was harvested, the protein was quantitated, and gelatin zymography was performed. In the U-87 glioma line, the invasion molecule MMP-2 was downregulated by treatment with 10 ng/ml

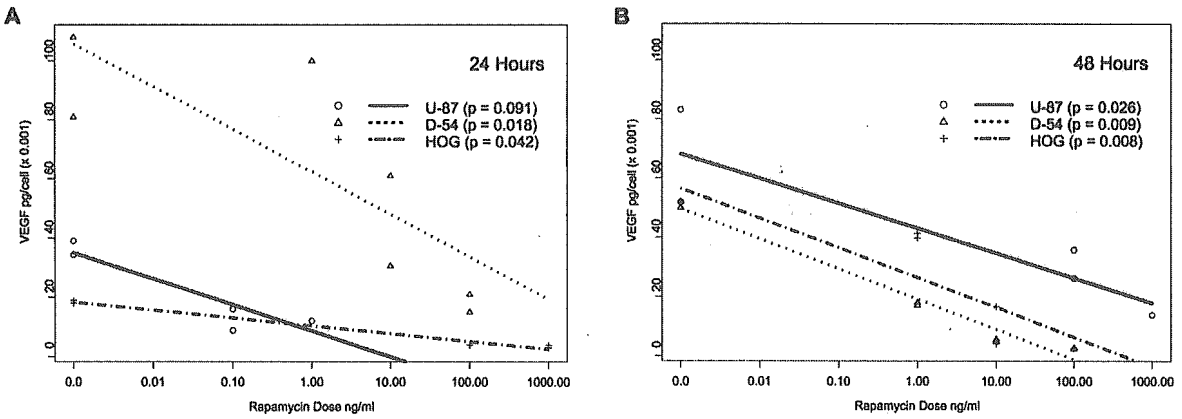

Fig. 2. Downregulation of VEGF in rapamycin-treated glioma cells. Glioma cell lines (D-54 and U-87) and HOG oligodendroglioma cells were treated with the indicated doses of rapamycin for 24 h (panel A) and 48 h (panel B), and their VEGF production was determined by ELISA assay. Diminished cell numbers were accounted for by calculating VEGF production per viable cell. The experiment was replicated in duplicate samples over two different time points with similar outcomes. A linear model relating the VEGF values to log dose, time, and cell line was used to include a three-way interaction as well as all nested two-way interactions. Residual analyses demonstrated that the model fit the data. The *P*-value for the three-way interaction was 0.05, that for the two-way interaction between dose and time was 0.47, that for dose and cell line was 0.033, and that between time and cell line was <0.0001.

of rapamycin; however, significant quantities of MMP-9 were not present in untreated cells. In the D-54 cell line, both MMP-2 and MMP-9 were present and downregulated by 100 ng/ml of treatment with rapamycin. In the HOG cell line, only MMP-2 was present, and it did not appear to be altered by treatment with 1000 ng/ml of rapamycin (Fig. 3).

To determine if rapamycin inhibits in vitro invasion, glioma cell lines were treated with rapamycin for 24 h. In the U-87 and D-54 cell lines, invasion was inhibited with rapamycin concentrations below the IC_{50}. In contrast, in the HOG cell line, even treatment with 1000 ng/ml of rapamycin failed to alter in vitro invasion (Fig. 4).

In Vivo Studies: Subcutaneous Model

Rapamycin suppresses growth of subcutaneous tumors. To determine if rapamycin was efficacious in the treatment of established tumors, subcutaneous U-87 tumors were treated with 1.5 mg/kg/day of rapamycin for 45 days. In 63% (n = 8) of established tumors treated with rapamycin, there was regression with no evidence of residual tumor at the conclusion of the experiment. In all U-87 tumors treated with PBS alone (n = 8), there was no evidence of regression, and all mice had large tumors at the conclusion of the experiment ($P < 0.05$) (Fig. 5).

Rapamycin inhibits in vivo VEGF. To verify that rapamycin downregulates VEGF production in vivo, we treated subcutaneous U-87 tumors for 45 days with 1.5 mg/kg/day of rapamycin. Subsequent immunohis-

Table 2. Flow cytometric analysis results showing downregulation of the invasion molecule MT1-MMP by rapamycin on U-87 and D-54 cells*

Cell Line	Rapamycin Dose (ng/ml)	% MTI-MMP Positive Cells
D-54	0	15.6
D-54	100	7.25
U-87	0	9.9
U-87	10	3.45
HOG	0	3.95
HOG	1000	8.43

* The cells were treated for 48 h with rapamycin. The cells were then incubated with an isotype control antibody or an MT1-MMP-specific antibody with an FITC-conjugated fragment of goat anti-rabbit IgG and analyzed by flow cytometry. Positive isotype control staining was less than 1.9%.

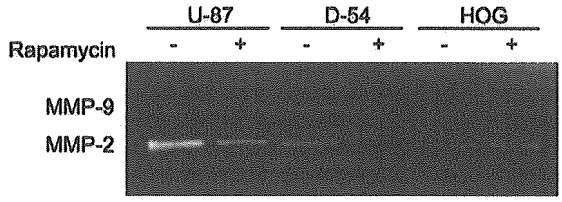

Fig. 3. Gelatin zymograph showing downregulation of the invasion molecules MMP-2 and MMP-9 by rapamycin. The glioma (U-87 and D-54) and oligodendroglioma (HOG) cell lines were treated for 48 h with rapamycin. The supernatant was harvested from each respective cell line, and 15 μg of protein from each supernatant was fractionated by gelatin zymography. Untreated (medium only) U-87 cells express MMP-2 but little MMP-9. U-87 cells treated with 10 ng/ml of rapamycin show MMP-2 downregulation. Untreated (medium only) D-54 cells express both MMP-2 and MMP-9. However, D-54 cells treated with 100 ng/ml of rapamycin demonstrated downregulation of both MMP-2 and MMP-9. Untreated (medium only) HOG cells expressed only MMP-2, and when this cell line was treated with the maximal dose of 1000 ng/ml of rapamycin, there was no change in MMP-2 expression.

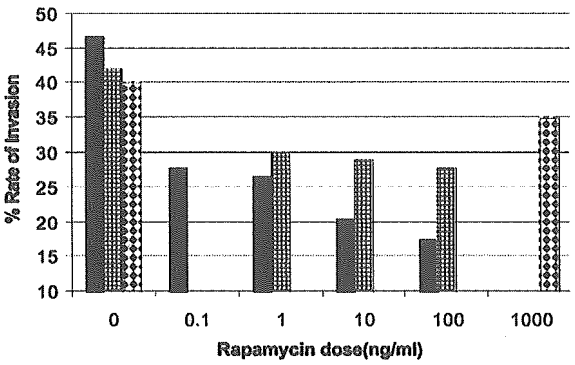

Fig. 4. In vitro invasion assay demonstrating that rapamycin inhibits invasion. U-87, D-54, and HOG cell lines were treated for 24 h with rapamycin. The glioma cells lines in 5% FCS were added at a concentration of 5×10^4 to the upper chamber, and 10% FCS was used in the lower chamber to induce cell migration. Rapamycin was added to the upper chamber at concentrations spanning the IC_{50}. Invasion was inhibited with rapamycin at concentrations less than the IC_{50} in both the U-87 and D-54 cell lines. However, even at 1000 ng/ml, rapamycin did not significantly inhibit the invasion of the HOG cell line. Solid bars, U-87; bars with small squares, D-54; white bars with black diamonds, HOG.

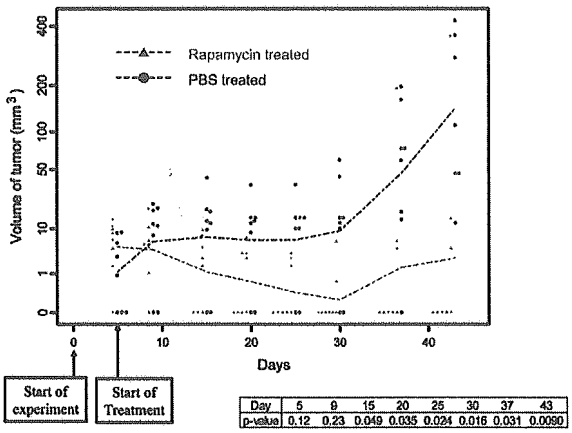

Day	5	9	15	20	25	30	37	43
p-value	0.12	0.23	0.049	0.035	0.024	0.016	0.031	0.0090

Fig. 5. Changes with time in the volume of subcutaneous U-87 tumors in nude mice with and without rapamycin treatment. Nude mice with established tumors (from subcutaneous injection of U-87 glioma cells) were treated daily with rapamycin at 1.5 mg/kg/day. There was regression in 63% (n = 8) of these tumors, with no evidence of residual tumor at the conclusion of the experiment (day 50) ($P < 0.05$). In contrast, all mice treated with PBS alone (n = 8) had large tumors at the conclusion of the experiment.

tochemical studies demonstrated that there was diminished VEGF production in tumors treated with rapamycin (Fig. 6). Determination of volumetric band density normalized to a maintenance protein (β-actin) on Western blot revealed that VEGF levels in tumors that were treated with rapamycin were lower (mean = 2.2; SD = 1.46) than those in tumors that were treated with PBS (mean = 5.3; SD = 1.27; $P = 0.037$) (Fig. 7). VEGF production did not appear to vary among the various tumor sizes in the PBS treatment group. Interestingly, the one rapamycin-treated U-87 tumor that achieved a size similar to the PBS-treated control tumors had a localized area of diminished VEGF production but had discrete areas of high VEGF production, possibly representing a mechanism of chemotherapy resistance. This tumor remained small volumetrically until day 30, at which point growth increased 60-fold in 15 days.

Rapamycin inhibits in vivo metalloproteinases. To determine if rapamycin modulated MMPs in vivo, subcutaneous U-87 tumors were treated with rapamycin and formalin fixed. Immunohistochemical staining failed to demonstrate dramatic changes in the level of MT1-MMP in U-87 tumors treated in vivo with rapamycin as compared to U-87 tumors treated with PBS. MT1-MMP staining was most prominent at the tumor periphery and appeared slightly more intense in U-87 tumors treated with PBS than in those treated with rapamycin (data not shown). Because MT1-MMP activity is necessary for the activation of proMMP-2, zymography was performed to identify the status of MMP-2 in U-87 tumors. Among rapamycin-treated subcutaneous U-87 tumors large enough to analyze 45 days after tumor implantation (n = 3), there was a marked reduction of MMP-2 (seen by gelatin zymography) as compared with the U-87 tumors treated with PBS alone (Fig. 8). The one rapamycin-treated tumor that escaped growth suppression did not show upregulation of MMP-2. These results are consistent with our in vitro data, thus confirming that rapamycin has an effect on MMPs.

In Vivo Studies: Intracranial Model

RAD001 fails to suppress orthotopic U-87 growth. Secondary to Novartis's interest in proceeding with a clinical trial for patients with malignant gliomas and since rapamycin has previously been demonstrated to be efficacious against established intracerebral xenografts, we elected to determine if RAD001 was efficacious in the treatment of established orthotopic U-87. Tumors were treated with 1.5 mg/kg/day or 5 mg/kg/day of the derivative of rapamycin, RAD001, starting three days after intracerebral implantation. In mice (n = 10/group) treated with 5 mg/kg or 1.5 mg/kg of RAD001 or with diluent, median survival was 30.5, 30.5, and 31 days, respectively, which was not statistically significant (data not shown). Three separate experiments produced similar results.

On quantitative Western blot analysis of orthotopically implanted U-87 tumors treated with RAD001, there was diminished p-4EBP1 (Fig. 1B). On immunohistochemistry, there was no discernable VEGF production within the intracerebral U-87 tumors, nor was there a difference with RAD001 treatment. Furthermore, Western blot analysis confirmed that there was no significant change in VEGF production. The intracerebral U-87 tumors treated with RAD001 demonstrated no significant changes in MMP-2 production on quantita-

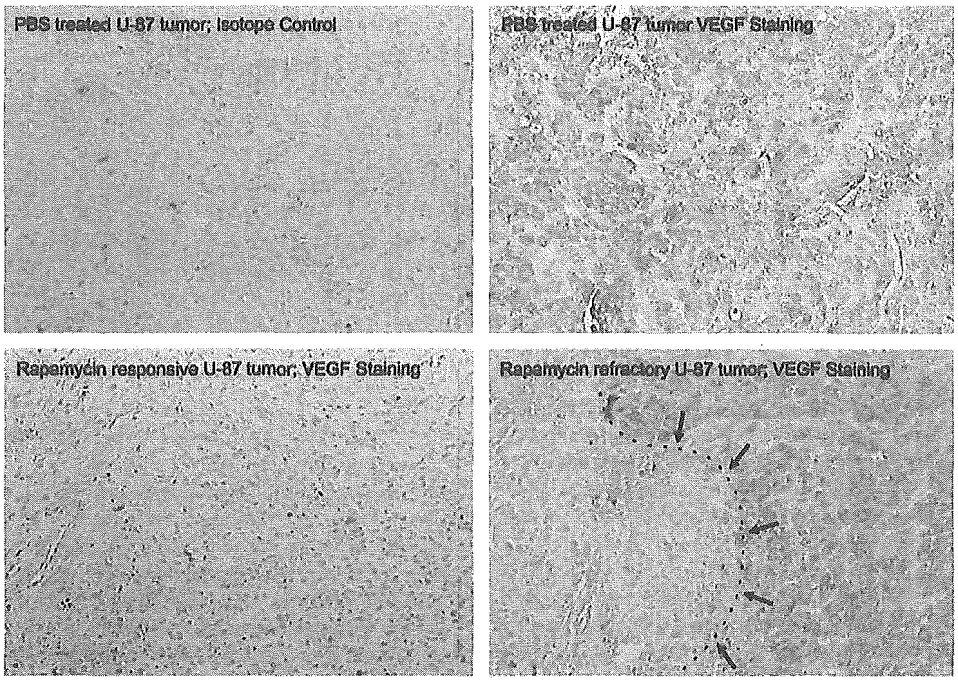

Fig. 6. Diminished immunohistochemical staining for vascular endothelial growth factor in subcutaneous U-87 cell tumors in nude mice after rapamycin treatment. Nude mice with established subcutaneous U-87 cell tumors were treated with rapamycin, and after 45 days of treatment, the experiment was terminated and the tumors were harvested. Paraffin-embedded sections of the tumors were stained with anti-VEGF antibody, and visualization employed the strepavidin-horseradish peroxidase system. In the lower right-hand panel, in the only U-87 tumor treated with rapamycin that attained a size similar to control-treated tumors, there was an area that was negative for VEGF staining (denoted by arrows), but the majority of the tumor demonstrated areas of high VEGF production (original magnification × 250).

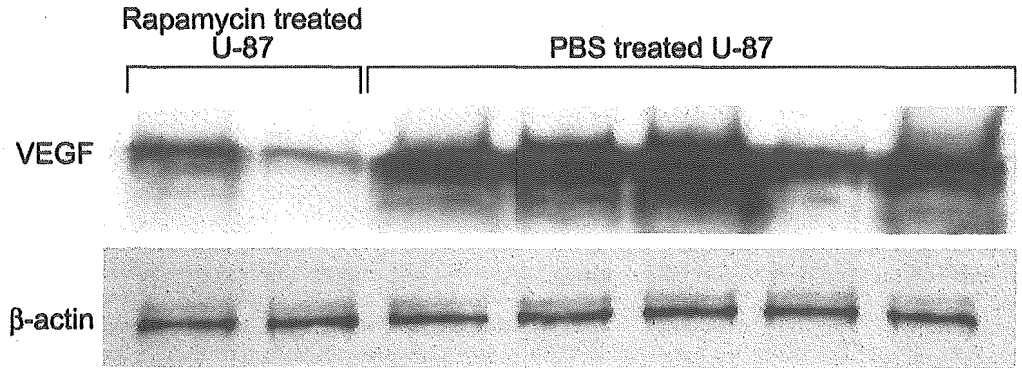

Fig. 7. Quantitative Western blot analysis demonstrating decreased VEGF production in vivo. Nude mice with established tumors (from subcutaneous injection of U-87 glioma cells) were treated daily with rapamycin at 1.5 mg/kg/day, and after 45 days of treatment, the tumors were harvested. The tumors were minced and underwent protein extraction. Equivalent amounts of protein extracts (20 μg/well) were subjected to 12.5% SDS-PAGE gel denaturing conditions and were immunoblotted with anti-VEGF and anti-β-actin. Fold increases in intensity of each band were scanned with a densitometer and normalized to control β-actin. Rapamycin inhibited VEGF production in vivo.

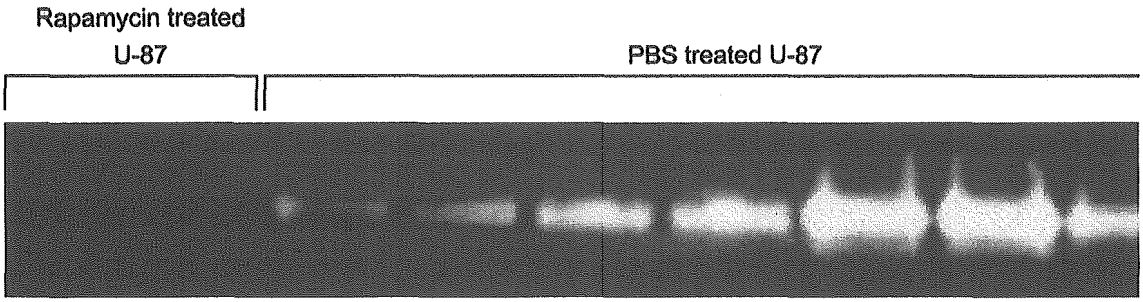

Fig. 8. Gelatin zymograph showing diminished production of MMP-2 in subcutaneous U-87 cell tumors in nude mice after rapamycin treatment. Nude mice with established subcutaneous U-87 cell tumors were treated with rapamycin, and after 45 days of treatment, the experiment was terminated and tumors were harvested. The tumor proteins were extracted and analyzed by gelatin zymography. Few rapamycin-treated U-87 tumors were of sufficient size to analyze (PBS-treated U-87 tumors were large and necrotic), but those that could be analyzed demonstrated diminished MMP-2 expression.

tive Western blot analysis or increased invasion characteristics by histology.

Discussion

One of the purposes of our study was to further elaborate on the mechanism of action of rapamycin so that salient molecular end point(s) could be identified for a clinical trial of rapamycin for glioma patients (Fig 9). These end points could include cytostasis, cell signaling, angiogenesis, and invasion. In this study we show that rapamycin or its derivative RAD001 not only works as a cytostatic agent by the accumulation of cells in the cell cycle G_1 compartment, with a corresponding decrease in the fraction of cells traversing the S phase, but also as an antiangiogenic (by inhibiting VEGF secretion) and an anti-invasion agent (by downregulating MT1-MMP, MMP-2, and MMP-9). Our data is consistent with findings of previously published studies indicating that mTOR-FRAP can regulate the activity of VEGF and invasion. Specifically, the signaling molecule mTOR-FRAP has previously been shown to be an upstream activator of HIF-1 (Hudson et al., 2002), and insulin has been shown to regulate HIF-1 action through PI3K/TOR-dependent pathways (Treins et al., 2002). The binding of HIF-1α to the VEGF promoter is a predominant enhancer of VEGF production (Fang et al., 2001; Tsuzuki et al., 2000), and rapamycin has been shown to inhibit the in vitro and in vivo production of VEGF (Brugarolas et al., 2003; El-Hashemite et al., 2003). In a recent article by Guba et al., rapamycin was shown to inhibit subcutaneous syngeneic adenocarcinomas by acting as an antiangiogenic agent by specifically inhibiting VEGF (Guba et al., 2002). Our studies confirm that downregulation of VEGF by rapamycin occurs in gliomas as well. In the VEGF ELISA, there was markedly diminished production of VEGF in all glioma cell lines, including the HOG cell line, in which rapamycin did not act in a cytostatic manner. Moreover, VEGF production was inhibited at rapamycin doses lower than the IC_{50}.

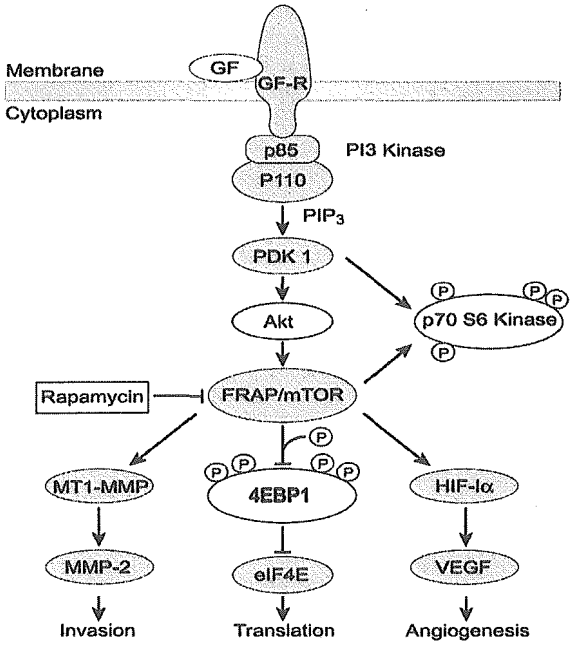

Fig. 9. Molecular targets of rapamycin. Activation of growth factor (GF) or cytokine receptors results in the sequential activation of PI3K, PDK1, Akt/PKB, and mTOR-FRAP. The tumor suppressor PTEN downregulates Akt activity (not shown). Rapamycin treatment of cells leads to the dephosphorylation (denoted by an encircled P) and inactivation of p70S6 kinase and 4EBP1. The dephosphorylation of 4EBP1 results in binding to eIF4E, which inhibits translation. Furthermore, the inhibition of mTOR-FRAP results in downregulation of HIF-1α and subsequent VEGF production. Finally, the inhibition of mTOR-FRAP also results in the downregulation of MT1-MMP, subsequent MMP-2 production, and resulting invasion.

Furthermore, in subcutaneous U-87 tumors, treatment with rapamycin resulted in diminished production of VEGF.

VEGF has been shown to upregulate several invasion molecules, such as MMP-2, MMP-9, and MT1-MMP (Rooprai et al., 2000), and insulin-like growth factor-1 has been shown to regulate MMP-2 and its MT1-MMP-mediated activation by the PI3K/Akt/mTOR pathway (Zhang and Brodt, 2003). In the U-87 and D-54 glioma cell lines, the invasion molecule MMP-2 and both MMP-2 and MMP-9, respectively, were downregulated with rapamycin. Additionally, flow cytometric analysis showed downregulation of MT1-MMP in U-87 and D-54 after 48 h of treatment. Treatment of the subcutaneous U-87 tumors with rapamycin in vivo also resulted in the downregulation of MMP-2. Therefore, treatment with rapamycin in vitro and in the subcutaneous model results in a cytostatic response with downregulation of MMPs and VEGF.

In contrast to the inhibition of tumor growth with rapamycin in the subcutaneous model, mice with established intracerebral U-87 tumors that were treated with RAD001 showed no increase in median survival. Our findings are in contrast to previously published data, which demonstrated a significant increase in median survival of mice with established intracerebral U-251 cells treated with rapamycin (Houchens et al., 1983). These differences may be secondary to as-yet-undefined differences between rapamycin and RAD001 or differences in the tumor models. The difference in efficacy in the subcutaneous and intracerebral models may be secondary to the intracerebral microenvironment, possibly due to influences on hypoxic response and neovascularization, which influences tumor response. Intratumoral p-4EBP1 was inhibited in those mice treated with RAD001, an indication that the concentrations of RAD001 used in vivo were able to inhibit the Akt pathway. Blouw et al. (2003) have shown that HIF-1α-knockout-transformed astrocytes have diminished growth in the vessel-poor subcutaneous environment resulting in severe necrosis as well as reduced growth and vessel density, whereas cells of the same type that are placed into the vascular-rich brain parenchyma have enhanced growth and invasion. Our data is consistent with this previously published report. By immunohistochemistry and quantitative Western blot analysis, the intracerebral U-87 tumors failed to show any appreciable levels of VEGF in vivo, which indicated that additional or alternative mechanisms are involved in VEGF regulation intracerebrally. Although rapamycin may inhibit signal transduction and/or cellular proliferation, the inhibition of HIF-1α may not be a desired strategy to treat astrocytomas since they may adapt to becoming more invasive and infiltrative (Blouw et al., 2003). However, we did not see evidence of increased invasion by histology or upregulation of MMP-2 on Western blot of RAD001-treated intracerebral U-87 tumors. Previously, Houchens et al. demonstrated an increase in median survival in mice with intracerebral U-251 tumors treated with rapamycin, which is in contrast to our data with intracerebral U-87. The difference in results may be, in part, due to differential dosing amount and interval of rapamycin administration, model systems, and/or the underlying molecular status of the tumors.

Given the lack of concordance between murine models and human efficacy, murine model systems are perhaps best utilized for establishing appropriate molecular end points, but these will require validation in human subjects. A proposed clinical trial could begin with a stereotactic biopsy to confirm the diagnosis and establish a baseline of the molecular targets, including p-4EBP1, VEGF, HIF-1α, and MMP-2. After administration of rapamycin or RAD001, the tumor could be removed for analysis of pharmacokinetic and drug-related molecular changes. In the scenario of treatment failure, re-resection or biopsy could establish definitely if failure is occurring through the HIF-1α/VEGF pathway. If this is a mechanism(s) of treatment failure, combination therapy with an anti-VEGF agent may be considered. In conclusion, our data suggest that clinical trials that incorporate only a limited molecular target such as a signal transduction molecule may not necessarily correlate with efficacy and will be inadequate to assess treatment failures and future combination chemotherapeutics.

Acknowledgments

We thank David M. Wildrick for editorial assistance, Hyung-Woo Kim for statistical analysis, and Jeffrey S. Weinberg and Mark R. Gilbert for thoughtful commentary. The oligodendroglioma cell line, HOG, was provided through the courtesy of Ken Aldalpe of The University of Texas M.D. Anderson Cancer Center.

References

Blouw, B., Song, H., Tihan, T., Bosze, J., Ferrara, N., Gerber, H.P., Johnson, R.S., and Bergers, G. (2003) The hypoxic response of tumors is dependent on their microenvironment. *Cancer Cell* **4**, 133–146.

Brugarolas, J.B., Vazquez, F., Reddy, A., Sellers, W.R., and Kaelin, W.G., Jr. (2003) TSC2 regulates VEGF through mTOR-dependent and -independent pathways. *Cancer Cell* **4**, 147–158.

Dilling, M.B., Dias, P., Shapiro, D.N., Germain, G.S., Johnson, R.K., and Houghton, P.J. (1994) Rapamycin selectively inhibits the growth of childhood rhabdomyosarcoma cells through inhibition of signaling via the type I insulin-like growth factor receptor. *Cancer Res.* **54**, 903–907.

El-Hashemite, N., Walker, V., Zhang, H., and Kwiatkowski, D.J. (2003) Loss of Tsc1 or Tsc2 induces vascular endothelial growth factor production through mammalian target of rapamycin. *Cancer Res.* **63**, 5173–5177.

Eshleman, J.S., Carlson, B.L., Mladek, A.C., Kastner, B.D., Shide, K.L., and Sarkaria, J.N. (2002) Inhibition of the mammalian target of rapamycin sensitizes U87 xenografts to fractionated radiation therapy. *Cancer Res.* **62**, 7291–7297.

Fang, J., Yan, L., Shing, Y., and Moses, M.A. (2001) HIF-1alpha-mediated up-regulation of vascular endothelial growth factor, independent of basic fibroblast growth factor, is important in the switch to the angiogenic phenotype during early tumorigenesis. *Cancer Res.* **61**, 5731–5735.

Guba, M., von Breitenbuch, P., Steinbauer, M., Koehl, G., Flegel, S., Hornung, M., Bruns, C.J., Zuelke, C., Farkas, S., Anthuber, M., Jauch, K.W., and Geissler, E.K. (2002) Rapamycin inhibits primary and metastatic tumor growth by antiangiogenesis: Involvement of vascular endothelial growth factor. *Nat. Med.* **8**, 128–135.

Houchens, D.P., Ovejera, A.A., Riblet, S.M., and Slagel, D.E. (1983) Human brain tumor xenografts in nude mice as a chemotherapy model. *Eur. J. Cancer Clin. Oncol.* **19**, 799–805.

Hudson, C.C., Liu, M., Chiang, G.G., Otterness, D.M., Loomis, D.C., Kaper, F., Giaccia, A.J., and Abraham, R.T. (2002) Regulation of hypoxia-inducible factor 1alpha expression and function by the mammalian target of rapamycin. *Mol. Cell Biol.* **22**, 7004–7014.

Lal, S., Lacroix, M., Tofilon, P., Fuller, G.N., Sawaya, R., and Lang, F.F. (2000) An implantable guide-screw system for brain tumor studies in small animals. *J. Neurosurg.* **92**, 326–333.

Lang, F.F., Gilbert, M.R., Puduvalli, V.K., Weinberg, J., Levin, V.A., Yung, W.K., Sawaya, R., Fuller, G.N., and Conrad, C.A. (2002) Toward better early-phase brain tumor clinical trials: A reappraisal of current methods and proposals for future strategies. *Neuro-Oncol.* **4**, 268–277.

Neshat, M.S., Mellinghoff, I.K., Tran, C., Stiles, B., Thomas, G., Petersen, R., Frost, P., Gibbons, J.J., Wu, H., and Sawyers, C.L. (2001) Enhanced sensitivity of PTEN-deficient tumors to inhibition of FRAP/mTOR. *Proc. Natl. Acad. Sci. USA* **98**, 10314–10319.

Price, D.J., Grove, J.R., Calvo, V., Avruch, J., and Bierer, B.E. (1992) Rapamycin-induced inhibition of the 70-kilodalton S6 protein kinase. *Science* **257**, 973–977.

Rooprai, H.K., Rucklidge, G.J., Panou, C., and Pilkington, G.J. (2000) The effects of exogenous growth factors on matrix metalloproteinase secretion by human brain tumour cells. *Br. J. Cancer* **82**, 52–55.

Schuler, W., Sedrani, R., Cottens, S., Haberlin, B., Schulz, M., Schuurman, H.J., Zenke, G., Zerwes, H.G., and Schreier, M.H. (1997) SDZ RAD, a new rapamycin derivative: Pharmacological properties in vitro and in vivo. *Transplantation* **64**, 36–42.

Sehgal, S.N., Baker, H., and Vézina, C. (1975) Rapamycin (AY-22,989), a new antifungal antibiotic, II. Fermentation, isolation and characterization. *J. Antibiot. (Tokyo)* **28**, 727–732.

Supko, J.G., and Malspeis, L. (1994) Dose-dependent pharmacokinetics of rapamycin-28-*N*,*N*-dimethylglycinate in the mouse. *Cancer Chemother. Pharmacol.* **33**, 325–330.

Treins, C., Giorgetti-Peraldi, S., Murdaca, J., Semenza, G.L., and Van Obberghen, E. (2002) Insulin stimulates hypoxia-inducible factor 1 through a phosphatidylinositol 3-kinase/target of rapamycin-dependent signaling pathway. *J. Biol. Chem.* **277**, 27975–27981.

Tsuzuki, Y., Fukumura, D., Oosthuyse, B., Koike, C., Carmeliet, P., and Jain, R.K. (2000) Vascular endothelial growth factor (VEGF) modulation by targeting hypoxia-inducible factor-1alpha→ hypoxia response element→ VEGF cascade differentially regulates vascular response and growth rate in tumors. *Cancer Res.* **60**, 6248–6252.

Zhang, D., and Brodt, P. (2003) Type 1 insulin-like growth factor regulates MT1-MMP synthesis and tumor invasion via PI 3-kinase/Akt signaling. *Oncogene* **22**, 974–982.

Clinical Chemistry 52:3
370–378 (2006)

Molecular Diagnostics and Genetics

Allelic Losses of Chromosome 10 in Glioma Tissues Detected by Quantitative Single-Strand Conformation Polymorphism Analysis

Nobuhiro Hata,[1,2] Koji Yoshimoto,[1] Nobuhiko Yokoyama,[1] Masahiro Mizoguchi,[1] Tadahisa Shono,[1] Yanlei Guan,[1,2] Tomoko Tahira,[2] Yoji Kukita,[2] Koichiro Higasa,[2] Shinji Nagata,[1] Toru Iwaki,[3] Tomio Sasaki,[1] and Kenshi Hayashi[2*]

Background: **Detection of loss of heterozygosity (LOH) in clinical tissue samples is frequently difficult because samples are usually contaminated with noncancerous cells or because tumor cells in single tissues have genetic heterogeneity, and the precision of available techniques is insufficient for reliable analysis in such materials. We hypothesized that single-strand conformation polymorphism (SSCP) analysis can precisely quantify the gene dosage in mixed samples and is suitable for detection of LOH in clinical tissue samples.**

Methods: **We assessed the accuracy of a fluorescent SSCP method for the quantification of single-nucleotide polymorphism (SNP) alleles, using DNAs that were composed of cancerous DNA mixed with noncancerous DNA at various ratios. We applied this method to precisely characterize LOH in glioma tissue samples, using 96 SNPs that were evenly distributed throughout chromosome 10.**

Results: **LOH could be detected even in the cancerous DNA heavily contaminated (up to 80%) with noncancerous DNA. Using this method, we obtained LOH profiles of 56 gliomas with resolution at the SNP level (i.e., 1.5-Mbp interval). Anaplastic astrocytomas exhibited both 10p and 10q LOH, whereas diffuse astrocytomas frequently (63% of the cases) exhibited loss of 10p alone. We also found a possible new LOH region (around 10p13) in gliomas.**

Conclusions: **The present method is effective for precise mapping of LOH region in surgically obtained tumor tissues and could be applicable to the genetic diagnosis of cancers other than gliomas.**

Loss of heterozygosity (LOH)[4] is a common genetic alteration in various kinds of cancer, and its detection is informative for diagnosis and prognosis *(1)*. In brain tumors, combined 1p and 19q LOH is a statistically significant predictor of both chemosensitivity and longer survival in patients with oligodendroglial tumors *(2, 3)*. In general, LOH is a genetic alteration that leads to the inactivation of tumor suppressor genes and is considered to be a critical event in cancer development *(4)*. Thus, mapping of LOH regions is a practical approach to the identification of genes whose loss is related to tumorigenesis *(5)*.

LOH on chromosome 10 is the most frequent genetic alteration in glioblastomas (GBMs), which are the most malignant grade of gliomas according to WHO criteria *(6, 7)*. Investigation of segmental LOH on chromosome 10 in GBMs has revealed at least 3 common LOH regions: 10p14–15, 10q23–24, and 10q25–26 *(8–14)*. It has therefore been suggested that multiple tumor suppressor genes exist on chromosome 10. The *PTEN* gene at 10q23 has been identified as a tumor suppressor gene in GBM *(15, 16)*. The significance of LOH in the other chromosome 10 regions, however, is still controversial. Thus,

Departments of [1] Neurosurgery and [3] Neuropathology, Graduate School of Medical Sciences, and [2] Division of Genome Analysis, Research Center for Genetic Information, Medical Institute of Bioregulation, Kyushu University, Fukuoka, Japan.

* Address correspondence to this author at: Division of Genome Analysis, Research Center for Genetic Information, Medical Institute of Bioregulation, Kyushu University, Maidashi 3-1-1, Higashi-ku, Fukuoka 812-8582, Japan. Fax 81-92-632-2375; e-mail khayashi@gen.kyushu-u.ac.jp.

Received September 25, 2005; accepted December 8, 2005.
Previously published online at DOI: 10.1373/clinchem.2005.060954

[4] Nonstandard abbreviations: LOH, loss of heterozygosity; GBM, glioblastoma; SNP, single-nucleotide polymorphism; SSCP, single-strand conformation polymorphism; LOQUS, LOH estimation by quantitative SSCP analysis; AA, anaplastic astrocytoma; DA, diffuse astrocytoma; and SSC, standard saline citrate.

detailed mapping of LOH regions is important to clarify the mechanism of malignant glioma formation.

Although conventional LOH studies have used allelotyping with microsatellite markers, these methods are not sufficient for the identification of specific genes because of the low density of the available markers. On the other hand, single-nucleotide polymorphisms (SNPs) are the most abundant form of sequence variations in the human genome *(17)*, and worldwide efforts to collect SNPs have led to the accumulation of millions of these polymorphisms in public databases. Because of their overwhelming abundance in the genome, SNPs can serve as the basis for a high-density LOH analysis method. Many SNP-genotyping methods have been developed, and some of them can be applied to detect LOH *(18, 19)*. A quantitative SNP genotyping method using an oligonucleotide array, called WGSA, detects LOH with high resolution. The detection rate of LOH, however, is lower for DNA samples extracted from heterogeneous tumor tissue because of contamination by nonmalignant cells *(20)*.

In gliomas, diffuse infiltration is frequently observed independent of histologic grade, and the tumor tissue is not demarcated from noncancerous tissue *(21)*. Tolerance to contamination by noncancerous cells is therefore essential for LOH analysis of glioma samples. We previously developed a SNP-genotyping method, PLACE-SSCP, in which PCR products are postlabeled with fluorescent dyes and labeled products are analyzed in an automated capillary electrophoresis system under single-strand conformational polymorphism (SSCP) analysis conditions *(22, 23)*. In this system, precise quantification of allele frequencies of SNPs is possible with use of pooled DNA samples *(24)*.

In the present study, we explored the effectiveness of PLACE-SSCP for detecting allelic imbalance and developed a new sensitive approach, LOH estimation by quantitative SSCP analysis (LOQUS), to detect LOH at the SNP resolution level. We first evaluated the high sensitivity of this analysis, using a tumor cell line DNA artificially mixed with DNA from noncancerous cells. Subsequently, we analyzed LOH on chromosome 10 in glioma samples and investigated the correlation between the LOH profile and histologic grade. This method revealed a new LOH hot spot at 10p13, which is a putative area that may harbor tumor suppressor genes.

Materials and Methods

SAMPLES AND DNA PREPARATION

Glioma samples were obtained from patients during surgery at Kyushu University Hospital or other affiliated institutions. A part of the tumor tissue was saved for histopathologic examination; the rest was snap-frozen in liquid nitrogen and stored at −80 °C. Tumors were histologically diagnosed by a qualified neuropathologist and graded according to the WHO criteria *(21)*. Tumor tissue samples were collected from 56 patients with gliomas, including 35 GBMs, 8 anaplastic astrocytomas (AAs), 8 diffuse astrocytomas (DAs), and 5 gliomas categorized as WHO grade I (3 pilocytic astrocytomas, 1 pilomyxoid astrocytoma, and 1 ganglioglioma). Among them, 13 GBMs were used in a previous study of LOH analysis with microsatellite markers *(25)*. Tumor DNA was isolated from the frozen blocks by a standard phenol–chloroform extraction procedure. Corresponding wild-type DNA was isolated from a blood sample from the same patient by use of a QIAamp DNA Blood Kit (Qiagen). The present investigation was approved by the Ethics Committee of Kyushu University.

SINGLE-NUCLEOTIDE POLYMORPHISMS

We chose 384 SNPs on chromosome 10 from public databases: JSNP (http://snp.ims.u-tokyo.ac.jp/), TSC (http://snp.cshl.org/), and NCBI dbSNP (http://www.ncbi.nlm.nih.gov/SNP/). The frequencies of the minor alleles for the chosen SNPs were >20% in Japanese or Asians in at least one of the above public databases. Among them, 288 SNPs were mapped to the distal portion of chromosome 10q (10q25-telomeric end), and 96 SNPs were from other regions of chromosome 10. The genomic sequences including the chosen SNPs were downloaded from NCBI (http://www.ncbi.nlm.nih.gov/), and the repetitive sequences were masked by use of *Repeatmasker* (http://www.repeatmasker.org/). PCR primer pairs for all SNPs were designed for the nonredundant regions by use of *Primer3* software *(26)* to obtain a product of 80 to 300 bp and a standardized primer melting temperature (T_m) of 55–65 °C. Oligonucleotide primer pairs (custom synthesized at SIGMA Genosys, Hokkaido, Japan) were made to carry either 5′-ATT or 5′-GTT for postlabeling purposes, as described previously *(22)*.

PCR

PCR was performed in a total volume of 5 μL containing 25 ng of template DNA, 0.25 μM each of the primers, 0.2 mM each of the nucleotides, 0.125 U of AmpliTaq® DNA polymerase (Applied Biosystems), 27.5 ng of TaqStart™ antibody (Clontech Laboratories), 2 mM $MgCl_2$, 10 mM Tris-HCl (pH 8.3), 50 mM KCl, and 50 nL/μL dimethyl sulfoxide. The thermal cycle profile was 1 min at 94 °C for initial heating, followed by 40 cycles of 30 s at 94 °C, 30 s at 60 °C, and 1 min at 72 °C.

PLACE-SSCP AND DATA ANALYSIS

Post-PCR labeling was performed, followed by removal of the residual fluorescent nucleotides by gel filtration, as described previously *(23)*. Electrophoresis was performed under SSCP conditions in a 36-cm capillary in the ABI Prism® 3100 genetic analyzer (Applied Biosystems). The samples were dissolved in 0.5 mmol/L EDTA, loaded by electrokinetic injection at 2 kV for 10 s, and separated at 15 kV for 30 min, as described previously *(27)*. Output data

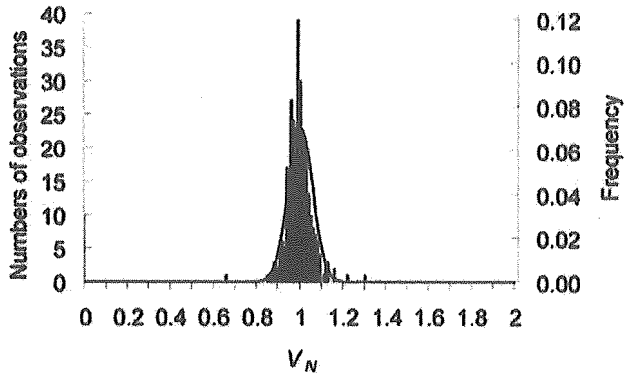

Fig. 1. Distributions of run-to-run variability of the peak-height ratio (V_N) of the 2 alleles in heterozygous samples.

The peak-height ratio (R_N) of every sample heterozygous for all SNPs was determined in duplicate runs. The ratio of R_N for the duplicates (V_N) was then calculated. *Columns* indicate the numbers of observed V_N within the bins of width (V_N) 0.05. The *curve* shows the approximated gaussian distribution, in which the mean (SD) was 1.000 (0.057).

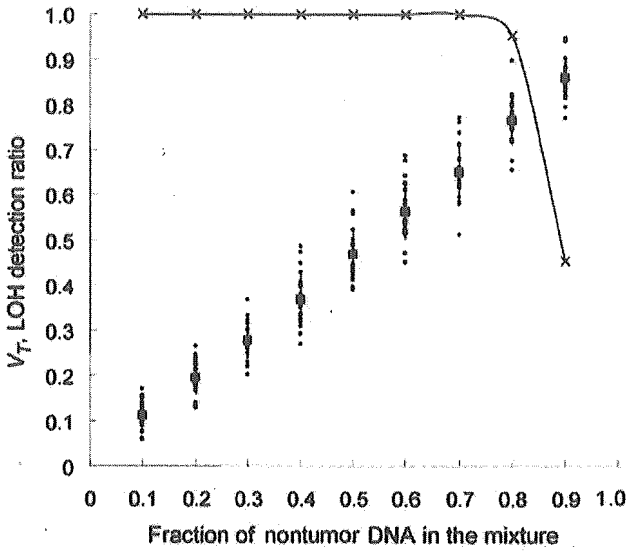

Fig. 2. LOH analysis using mixed samples.

The *x axis* shows the fraction of nontumor DNA in the mixture. The *y axis* shows V_T value or LOH detection rate. Each ● represents V_T for each locus (22 loci) across the 9 different mixing ratios. ■ and *vertical lines* indicate mean (SD) values of V_T. × indicate LOH detection rates, which were determined as the fraction of SNPs for which V_T was <0.83. See text for the definition of V_T.

were converted to ASCII format and then imported to Quantitative Interpretation of SSCP in Capillary Array (QUISCA) software for analysis *(23, 28)*.

DNA FOR MIXING EXPERIMENT

We purchased DNA samples extracted from a non-small lung cancer cell line (NCI-H2126) and its matched non-cancer cell line (NCI-BL2126) from the American Type Culture Collection. The DNA concentrations were determined by use of a PicoGreen ds-DNA quantification assay (Molecular Probes), and paired DNA of equal concentration was obtained by diluting with 0.1× Tris-EDTA buffer. The tumor DNA was then diluted with NCI-BL2126 DNA of the same concentration in 10% increments.

FLUORESCENT IN SITU HYBRIDIZATION

Imprint preparations of tumor cells were prepared from unfixed snap-frozen samples, as described previously with some modifications *(29)*. In brief, small pieces of cancer tissue were touched against silanized slides, and the slides were fixed 3 times in methanol–acetic acid (3:1 by volume) for 10 min each and subsequently air-dried. Cells on slides were denatured in 700 mL/L formamide in 2× standard saline citrate (SSC; pH 7) at 75 °C for 5 min. After dehydration in an ethanol series (700 mL/L, 850 mL/L, and absolute ethanol), samples were treated with 0.1 g/L proteinase K (Merck) in phosphate-buffered saline (pH 7) at 37 °C for 3 min, followed by a second dehydration in ethanol. Hybridization was performed with the LSI PTEN/CEP 10 Dual Color Probe, which is a mixture of a locus-specific probe (LSI) localized on band 10q23 and a subcentromeric probe (CEP) on band 10p11.1-q11.1 (Vysis). The probe mixture was denatured at 73 °C for 5 min and hybridized to the denatured cells on the slides. After cells were covered with an 18 × 18 mm coverslip and sealed with rubber cement, hybridization was allowed to proceed for 2 days. Slides were then washed twice at room temperature for 5 min in 2× SSC containing 3 mL/L NP-40, then at 73 °C for 2 min. After washing, nuclei were counterstained with 0.15 mg/L 4.5-diamino-2-phenyl-indole. Slides were scored for the number of fluorescent signals in each nucleus by use of a Zeiss Axioskop 2 plus fluorescence microscope equipped with a triple-pass filter (Aqua/Green/Orange; Vysis).

MICROSATELLITE ANALYSIS

Tumor and nontumor DNAs were evaluated by a PCR-based LOH assay using 8 microsatellite markers located at regions on chromosome 10 frequently deleted in gliomas (D10S591, D10S1649, D10S1652, D10S1765, D10S587, D10S216, D10S217, and D10S1655). PCR and fluorescence labeling were performed according to a previously described method *(25)*. Capillary electrophoresis was performed with a 310 Prism Genetic Analyzer (Applied Biosystems). Raw electrophoresis data were analyzed with GeneScan Analysis software (Applied Biosystems). Allelic status was assessed based on the criteria established in a previous study *(25)*. Microsatellite instability was determined by the appearance of extra bands on tumor DNA examination.

Results

SELECTION OF SNP MARKERS

We tested the effectiveness of PLACE-SSCP by assessing the LOH status of chromosome 10, which is the site of one of the most frequent genetic alterations associated with malignant gliomas *(6, 7)*. We first chose 384 SNP markers

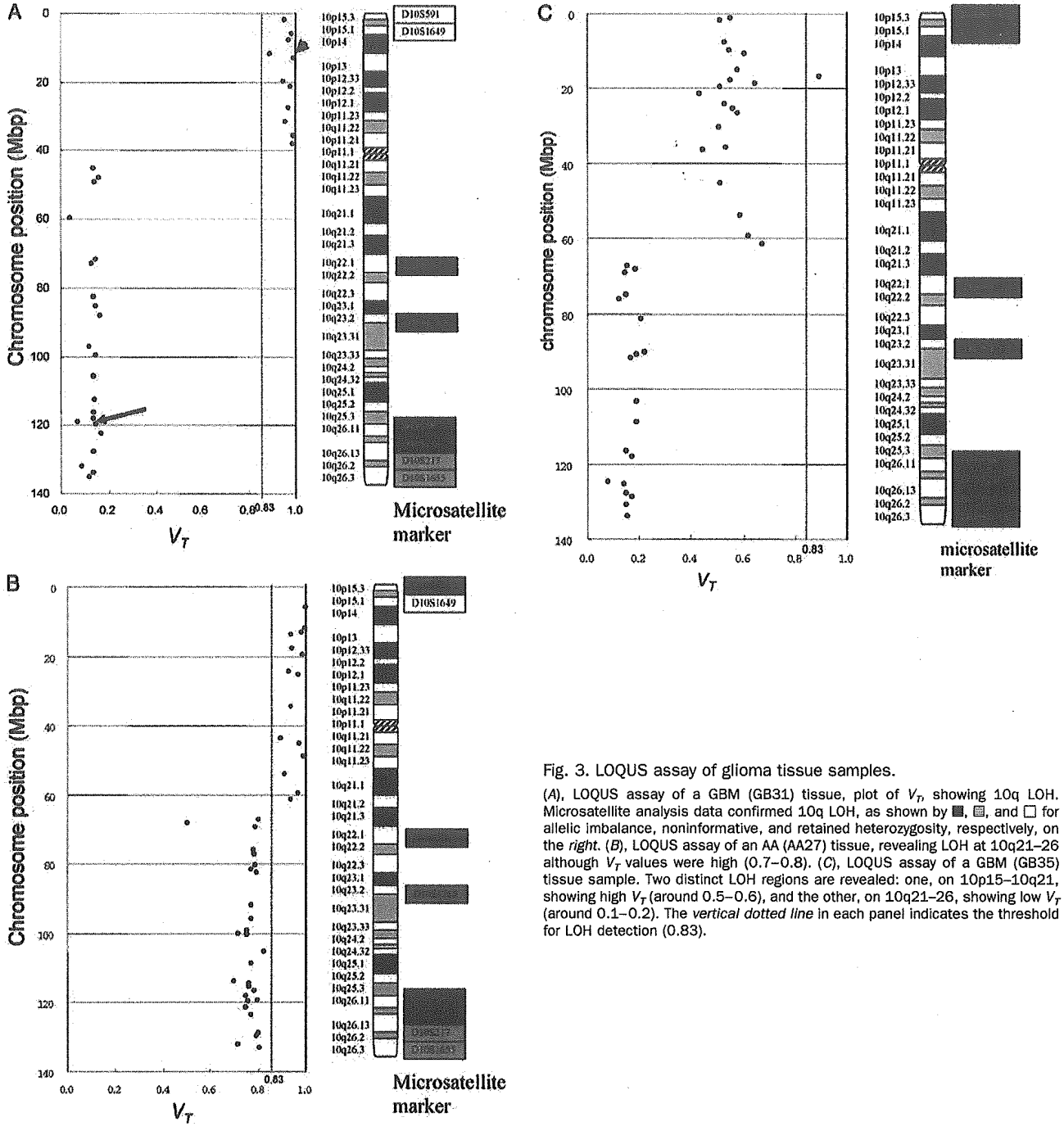

Fig. 3. LOQUS assay of glioma tissue samples.

(*A*), LOQUS assay of a GBM (GB31) tissue, plot of V_T, showing 10q LOH. Microsatellite analysis data confirmed 10q LOH, as shown by ■, ▤, and □ for allelic imbalance, noninformative, and retained heterozygosity, respectively, on the *right*. (*B*), LOQUS assay of an AA (AA27) tissue, revealing LOH at 10q21–26 although V_T values were high (0.7–0.8). (*C*), LOQUS assay of a GBM (GB35) tissue sample. Two distinct LOH regions are revealed: one, on 10p15–10q21, showing high V_T (around 0.5–0.6), and the other, on 10q21–26, showing low V_T (around 0.1–0.2). The *vertical dotted line* in each panel indicates the threshold for LOH detection (0.83).

on chromosome 10 as described in the *Materials and Methods*, and PCR reactions on tumor and corresponding nontumor DNA were performed for each sequence-tagged site containing a SNP in the same batch. Subsequently, PCR products were divided and used for sequencing and PLACE-SSCP analyses for the same 8 individuals, and these data were interpreted independently. Among the 384 SNPs, a total of 70 (18.2%) were excluded from further analysis because the peak patterns of the SSCP analyses were not interpretable (22 SNPs), separation of allele peaks of heterozygous samples was insufficient for quantitative SSCP analysis (28 SNPs), or there was no heterozygote sequenced among the 8 individuals (20 SNPs). From the remaining 314 SNPs, we excluded SNPs with a minor allele frequency <30% in the 8 individuals. The 96 SNPs that distributed evenly throughout chromosome 10 (marker intervals ~1.5 Mbp) were used for subsequent analyses.

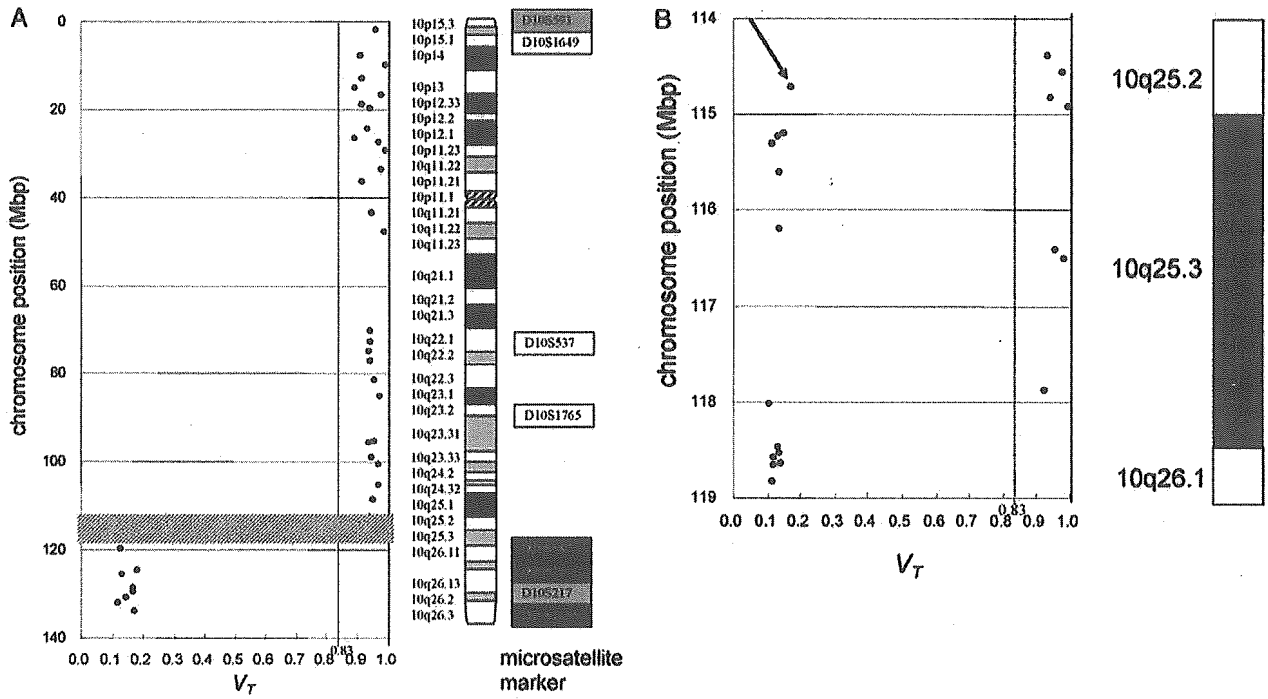

Fig. 4. LOQUS assay of an AA sample (AA24).

(*A*), LOH at a region distal to 10q, obtained with the set of 96 SNPs. is shown (*B*), *hatched region* in *A* (from 114 to 119 Mbp of chromosome 10) was analyzed further by use of high-density SNPs. There is a single LOH locus, rs720785 (*arrow*), at chromosome position 114 711 558 bp, disrupting the 2 regions of retained heterozygosity, indicating the presence of an LOH region <250 kbp in length. Another LOH region of ~1.5 Mbp on the chromosome region around 116 Mbp was also detected. The *vertical dotted line* in each *panel* indicates the threshold for LOH detection (0.83).

REPRODUCIBILITY OF PEAK-HEIGHT RATIOS OF ALLELES IN NONTUMOR CELLS FROM PERSONS HETEROZYGOUS FOR SNPs

The sensitivity of LOH detection by PLACE-SSCP depends on the accuracy of the estimation of relative allele abundance in the samples, which in turn depends on the reproducibility of peak-height ratios of alleles in either nontumor cells from individuals heterozygous for the SNP being evaluated or in tumor samples. We defined R_N as the height ratio of the peak for the first allele peak to the peak for the second allele in nontumor DNA from individuals heterozygous for each SNP. For each SNP, PCR reactions from the same DNA were performed in 2 wells of the same microtiter plate, and 2 R_N values (R_{N1} and R_{N2}) were obtained for all SNPs in nontumor cells showing heterozygosity. We analyzed the 96 SNPs, using nontumor DNA from 8 heterozygous individuals, and determined the variability of the peak-height ratio obtained for the same nontumor DNA (V_N) by R_{N1}/R_{N2} for all SNPs showing heterozygosity (326 determinations). The mean (SD) V_N was 1.000 (0.057), with a CV of 5.7%, and the data were fitted to a gaussian distribution by use the Shapiro–Wilk *W* test with JMP software (Ver. 5.0.1J; SAS Institute; http://www.sas.com/; Fig. 1) (*30*). The test revealed a gaussian distribution (W = 0.9626) with high significance (P <0.0001). We define V_T [min(R_T/R_N, R_N/R_T)] as an indicator of the fraction of the DNA with allelic imbalance in the tumor sample, where R_T is the peak height ratio of the tumor sample (see Fig. 2 of the Data Supplement that accompanies the online version of this article at http://www.clinchem.org/content/vol52/issue3/). We thus conclude that V_T <0.83 (3 SD from the mean) can be regarded as an LOH at a confidence level of ~99.7% (according to the probability density of the gaussian distribution). We adopted this criterion as an indication of LOH in the LOQUS assay described below.

MIXED DNA EXPERIMENT

Glioma tissue samples frequently show heterogeneity or infiltration by noncancerous cells. To further estimate the sensitivity of LOQUS to detect the allelic status in such situations, we performed reconstitution experiments in which a pair of DNA samples from tumor and healthy tissues of the same individual were mixed at various ratios and subjected to LOQUS analyses. The DNA samples for this experiment were obtained from a lung cancer cell line (NCI-H2126) and its matched noncancer cell line DNA (NCI-BL2126), in which LOH was detected in all informative microsatellite markers examined on chromosome 10 (*31*). Among the 96 SNPs, SSCP analysis of NCI-BL2126 indicated heterozygosity for 22. The LOQUS assay performed with these SNPs indicated that V_T increased proportionally in response to an increase in nontumor DNA (Fig. 2). At a mixing ratio of 20 (i.e., 20% tumor DNA and 80% nontumor DNA), LOH was detectable in 95% of the examined SNPs (21 of 22), and above